# 5 Use of Non-Invasive Ion-Selective Microelectrode Techniques for the Study of Plant Development

Joseph G. Kunkel,[1] Sofia Cordeiro,[2] Yu (Jeff) Xu,[1] Alan M. Shipley,[3] José A. Feijó[2]

## 5.1 Ion dynamics in plant development

Ion fluxes across membranes are known to have important biological roles. They exert their effect by two means: generating electrical fields and changing the local ion concentrations, thus affecting physiological processes that are dependent upon them.

Electrical fields exert force on charged particles, from molecules to organelles, and this has been proposed to lead to the movement of membrane proteins or cytoplasmic vesicles by field orientation, electrophoresis or electro-osmosis. On the other hand, cells react to the ions that carry these currents, many of which act via signal transduction pathways. If these ions have a catalytic or regulatory function, the biochemical consequences of any change in their concentration can be enough to trigger a response (Harold and Caldwell 1990; Feijó et al. 2004). Furthermore, accumulating evidence has shown that polarity, morphogenesis and many developmental steps in plant cells are defined by an intricate network of processes that often include ion distribution and concentration as major correlates. These phenomena are available for experimental manipulation and measurement during which one can seek evidence for causal relationships.

## 5.2 Molecular basis of ion fluxes in plants

Ionic equilibrium in plant cells is achieved, on the one hand, by the maintenance of an electrochemical gradient by proton ATPases on the plasma membrane (P-ATPases) and, on the other hand, by the flux of other ions, namely potassium, calcium and chloride through ion channels and transporters.

Turgor and volume regulation, two crucial parameters in plant physiology and development, are good examples of processes that are strictly dependent

[1] Department of Biology, University of Massachusetts Amherst, MA 01003-5810, USA

[2] Centro de Biologia do Desenvolvimento, Instituto Gulbenkian de Ciência, PT-2780-156 Oeiras, Portugal (e-mail: jfeijo@fc.ul.pt)

[3] Applicable Electronics Inc., Forestdale, MA 02644, USA

Plant Electrophysiology – Theory & Methods (ed. by Volkov)

upon ion regulation. Intracellular pressure in plant cells is achieved and maintained by the intracellular accumulation of ions and solutes, and their partition and sequestration in different osmotic biochemical forms in the vacuole (e.g. formation of salts or polymers). The turgor pressure thus created is required for cell expansion, elongation, gas exchange, transport of ions and solutes, etc.

Pivotal in the regulation is also the activity of the vacuolar proton ATPases (V-ATPases), much different from their plasma membrane counterparts both in structure and mechanism. Vacuolar pyrophosphatases (PPases) are a third active transport party in the system. The coordinated action of these three pump systems maintains the cytosol at a fairly constant and neutral pH, while keeping both vacuole and external apoplast acidic.

These pumps are the active source of energy for a number of channels and transporters (e.g. Sanders and Bethke 2000; Taiz and Zeiger 2002; Blatt 2004), many now well characterized as expressed in a number of tissues, evidenced by transcriptomics (e.g. Pina et al. 2005).

The particular ionic environment created by these conditions is cause and consequence of the ion fluxes across the cell's membranes, requiring tight regulatory mechanisms that keep calcium concentration low, potassium high and a pH neutral, among other homeostatic regulations (reviewed by Feijó et al. 1995; Holdaway-Clarke and Hepler 2003).

The study of plant ion dynamics is therefore of the utmost importance, and several laboratories have taken advantage of non-invasive microelectrode techniques, in particular scanning ion-selective probes, to approach it.

## 5.3 Scanning probe: technical advantages and disadvantages

In the past, we have reviewed the application of both voltage sensitive and ion-selective probes for the scanning of membrane domains underlying the development of plants, with special emphasis on a very specialized cell, the pollen tube (Shipley and Feijó 1999; Fig. 7C, D). To date, the pollen tube is probably the best-studied system in terms of ion fluxes, and the matter has been reviewed both for its occurrence and biological meaning (Feijó et al. 2001, 2004; Holdaway-Clarke and Hepler 2003). The reason for this specific cluster of applications lies in the absence of real alternatives to an extracellular scanning probe for use with plant cells. The analysis of ion fluxes in living cells has been accomplished through the use of invasive techniques such as impalement and patch clamp. These approaches usually allow one independent sample location per cell. Further sampling proceeds at the risk that prior sampling had an effect on the cell. Although results from these techniques have been remarkably important for the characterization of ion channel properties and activity in plant development, they are compromised by serious disadvantages. Since access to the plasma membrane is necessary for the

formation of a tight seal between the membrane and the patch pipette (giga-ohm seal), the plant cell wall has to be either enzymatically digested or mechanically removed, creating protoplasts. Both processes can alter plasma membrane properties, namely activity of membrane proteins, and more importantly induce a condition of stress that will likely hinder many underlying physiological processes. Moreover, the success rate of giga-ohm seal formation in plant protoplasts is generally low, which is probably caused by incomplete cell wall removal or immediate regeneration of a new cell wall. The use of extra-cellular vibrating or stepping probes, totally non-invasive methods, adds an important edge to the study of living cells.

Non-invasive scanning probes have gone through a series of transformations in use by diverse research groups.

One of the first vibrating calcium-selective electrode recording system was built, for the initial use of Jaffe and Levy (1987), as a direct coupled (DC) device by A.M. Shipley and C. Scheffey at the National Vibrating Probe Facility (MBL, Woods Hole).

The head stage used an AD515L chip with a 10 × gain fed to an AD524 amplifier set to 100 × gain with a DC offset control to cancel the Nernst potential on the ion-selective microelectrode. All measurements were referenced to an Ag-AgCl wire in a 3 M KCL salt bridge placed in the solution, millimeters away from the artificial calcium source. The microelectrode was vibrated at frequency of 0.5 Hz using a bench-top square-wave oscillator signal damped with an R/C network to smooth the vibratory movement of the microelectrode.

This original design was programmed in Pascal by Scheffey and it used a 60 Hz sampling routine to filter out line noise. This system measured the actual DC voltages (Nernst potential) across a ion selective liquid ion exchanger (LIX) column in the tip of a glass microelectrode positioned with a manual micromanipulator. Later a capacitively coupled (AC) device, introduced as described by Kühtreiber and Jaffe (1990), which "vibrated" between and paused at two extremes of a straight path. The system was controlled by a PC based Visual Basic computer program, DVIS written by W. Kuhtreiber. Vibration was via Burleigh piezopushers driven by an oscillator circuit. This AC design does not measure the actual voltage at the points of measurement and has efficiency properties based on both the LIX used and the circuit's capacitor that accumulates the voltage change. Using a capacitor, the efficiency of the system varies depending on the magnitude of voltage measured. This "self-referencing" AC system uses a continuous oscillation and the probe takes a few oscillations for overcoming hysteresis, a phenomenon whereby a circuit's current properties depend upon its past history, and become stable. Then the software accumulates a rolling average of the cyclical measurements. When a capacitor starts out it is uncharged; as it is oscillated in a field then its first oscillation starts with no charge and a few cycles of oscillation (discharge in one direction and recharge in the opposite direction) must occur before the charge on the capacitor has a symmetrical history comparing opposite polls of oscillation. Thus, at least the first hemi-oscillation must be dropped as not

equivalent to the next hemi-oscillations. In addition the early approach of using a rolling average creates statistical and instrumental strategy problems. Notably, the first available stable datum from this approach comes on the *k+1* oscillation, where *k* is the rolling average base number. This error-laden protocol contributed to several important papers on tip growing systems (Kühtreiber and Jaffe 1990; Schiefelbein et al. 1992). At this point, a division in measurement philosophy occurred with part of the groups returning to the DC device because of its potential as a more comprehensive approach and reliable measurement efficiency. Table 5.1 lists the dynamic efficiencies estimated for the DC coupled electrodes listed which were achieved by using the continuous stepping approach, SIET. These efficiencies were improvements over those achieved with the AC devices and were listed elsewhere (www.bio.umass.edu/biology/kunkel/nvp_cali.html). Unfortunately, this table of efficiencies was assumed to apply to all oscillating ion-selective probes and often AC device results were published without benefit of accurate efficiency estimates. This is a major problem for the AC devices, since there is no adequate approach to establishing the AC system's dynamic efficiencies. In the few measurements of the dynamic efficiency of the calcium LIX using the AC devices driven at identical Hz at the National Vibrating Probe Facility, the dynamic efficiency was substantially lower than with the DC amplifier. Using the DC device and software improvements to the DVIS software, it was possible to eliminate rolling averages that created correlations between adjacent measurements, making it a bad experimental design. Rolling averages were replaced with statistics on independent unit measurements and this approach was used in further tip growth studies (Holdaway-Clarke et al. 1997; Feijó et al. 1999; Cardenas et al. 2000). Since the idea is to detect specific ion concentration as a function of DC voltage change on a LIX microelectrode, it is crucial to accurately detect the microelectrode's DC voltage at each extreme of the movement excursion. Fundamentally, these systems are concentration meters that derive ion flux or movement as a function of the local ion concentration difference measured between two positions close to a membrane. To accomplish this, the SIET (scanning ion-electrode technology) system was developed (Shipley and Feijó 1999). A major change in measurement protocols with this DC device allows for faster, multidimensional- and multi-probe measurements. ASET (automated scanning electrode techniques) software, developed by E. Karplus, (Science Wares, E. Falmouth, Mass., USA) established the sampling-rule approach to measurement. The sampling rule defines a set of unit measurements that can be as simple as a stationary measurement at one point with one probe, or as complicated as three-dimensional flux measurements involving stepping in the micrometer range of differential distances to measure differential concentrations with multiple probes, whether voltametric, amperimetric or both. Statistics on sampling is accomplished by replicating sampling rule unit measurements using standard experimental designs and controlling the pattern of unit measurements via interactive software-defined patterns of sampling sites. Complications of hysteresis are avoided in the DC sampling rules because the symmetry of oscillatory

**Table 5.1.** Dynamic calibration of ion selective micro-electrodes. All dynamic efficiencies were determined using DC methods. Dynamic efficiencies while continuously oscillating (*Step eff%*) were determined using the older 3DVIS software initially written by WielKuhtreiber and modified for 3D measurements by J.G. Kunkel. Dynamic efficiencies based on sampling rules (*Rule eff%*) were determined using the newer ASET software from ScienceWares. For convenience to the reader, we list the technical parameters of each ion listed (diffusion coefficient at infinite dilution, $D_o$; valence, i and Nernst slope) as well as the LIX used and its 90% response time. The Hz quoted refers to the stepping frequency used in the older 3DVIS software. The bicarbonate diffusion coefficient is listed for the carbonate LIX because at physiological pHs the carbonate travels mainly in the bicarbonate form

| Ion | Do | i | Nernst slope | LIX | t90 | Hz | Step eff% | Rule eff% |
|---|---|---|---|---|---|---|---|---|
| $K^+$ | 19.6 | 1 | 58 | Fl:K IB | <1 s. | 0.3 | 70% | 85% |
| $H^+$ | 93.7 | 1 | 58 | Fl:H IIA | ~0.6 s | 0.3 | 80% | 100% |
| $Ca^{+2}$ | 7.9 | 2 | 29 | Fl:Ca IIA | <5 s | 0.3 | 50% | 80% |
| $Mg^{+2}$ | 7.1 | 2 | 29 | Fl:Mg IV | <30 s | 0.25 | 30% | na |
| $Cl^-$ | 20.3 | −1 | −58 | IE:170 | na | 0.5 | 85% | 100% |
| $CO_3^{-2}$ | 13.9 | −2 | −29 | IE:310 | na | na | na | 40% |

(differential) data does not intrude on the collection process. As a result, a substantial improvement of the dynamic efficiency is achieved for the DC sampling rule approach for all LIXes tested, as indicated in Table 5.1. It must be emphasized that establishment of the dynamic efficiency of the electrodes must be determined case-by-case within the context of a given sampling rule (cf. Table 5.2). Dynamic efficiency will vary with the length of waiting time for

**Table 5.2.** A sampling rule for a dual probe system. *Point name*: probe position names as shown in Fig. 5.1, e.g. "$H^+_{(1)}$" refers to $H^+$ probe in location 1; dX, dY, dZ: displacements (µm) in X,Y,Z dimensions respectively to get to their corresponding point name; *WaitSec* defines a waiting time in seconds at the point name; *AvgSec* seconds averaging at 1000 measurements per second. The probe tips were placed 40 µm apart in the Y dimension. The movement to each new location is accomplished in less than 0.1 s and is included in the WaitSec parameter so that the entire time for the dual probe 3-D unit sample to be taken is the sum of WaitSec and Avgsec=9.2 s

| Point name | dX | dY | dZ | WaitSec | AvgSec |
|---|---|---|---|---|---|
| $H^+_{(1)}$ | 0 | −20 | 0 | 0.8 | 0.5 |
| $O_{2(1)}$ | 0 | 20 | 0 | 0.5 | 0.5 |
| $H^+_{(2)}$ | 10 | −20 | 0 | 0.8 | 0.5 |
| $O_{2(2)}$ | 10 | 20 | 0 | 0.5 | 0.5 |
| $H^+_{(3)}$ | 0 | 10 | 0 | 0.8 | 0.5 |
| $O_{2(3)}$ | 0 | 30 | 0 | 0.5 | 0.5 |
| $H^+_{(4)}$ | 0 | −20 | 10 | 0.8 | 0.5 |
| $O_{2(4)}$ | 0 | 20 | 10 | 0.5 | 0.5 |

LIX wobble to subside, length of probe integration of the signal, the properties of the LIX used and other factors. For instance, the strength of the buffer can dramatically influence the apparent flux of protons (Faszewski and Kunkel 2001). The 100% dynamic efficiency achieved with the DC sampling rule approach (Table 5.1) applies only to low- or un-buffered samples. With low buffer levels secretion of enough protons to clear the local culture media of effective buffer must occur, otherwise the buffer extinguishes protons as they are secreted and the probe has effectively no difference in concentration to measure (Kunkel et al. 2001). Use of traditional bicarbonate buffered culture media such as Holtfretter's solution will result in a substantial loss of efficiency (efficiency=63%) in measuring protons. Doubling the bicarbonate buffer in the Holtfreter's, results in a reduction in efficiency to 43% (Faszewski and Kunkel 2001). This example points clearly to the need of examining probe manuscripts with respect to their reliable dynamic calibrations for the specific conditions used.

The SIET approach is especially suited to development involving growth or morphogenesis of a cell or tissue. This is because the microelectrode can be non-invasively moved around the extracellular medium surrounding a specimen, thus allowing large spatial coverage, as well as tracking a modulating or growing point.

These non-invasive extracellular methods provide complimentary information to add to intracellular methods using fluorescent reporting molecules (e.g. Holdaway-Clarke et al. 1997). In their most ambitious applications with adequate calibration, non-invasive ion probes can be used to integrate the relatively steady ionic fluxes emanating from a region or unit surface area of a cell or cellular membrane (Cardenas et al. 1999, Fig. 8F). Often a probe has been used in a semi-quantitative way to observe relative ion flux spatial patterns focusing on temporal oscillatory patterns without calculating flux at other than the probe position in one dimension or extrapolating the flux to the cell surface (Holdaway-Clarke et al. 1997; Cardenas et al. 1999; Feijó et al. 1999; Zonia et al. 2001, 2002; Fig. 5.8E). Ion-selective probe calibration is essential to quantitative applications in which the properties of a particular region of a cell are of interest (Cardenas et al. 1999, Fig. 5.8F), or where the measurements are of importance in relating components of a model to one another (Feijó et al. 2001). The calibrations include simple calibration of the probe according to the Nernst equation [1]:

$$V = V_0 - (RT/zF) \cdot \ln(H/HA) \quad (1)$$

as well as determining the efficiency of the dynamic process of measuring the voltage difference between two points. In the later efficiency determination, there is a trade-off between allowing any probe wobble to come to rest after a move to a new location, the speed of the LIX to respond to the new location, the length of data collection, repetition of the measurement and how many other points one wants to measure in an experiment. Patterns of measurements that

include long movements between their starting positions require longer wait states to allow LIX wobble to subside. LIX wobble does not cause a decrease in efficiency; rather, it creates random noise resulting in outlier data. For that reason, more weight must be given to wobble suppression (via longer wait states) versus longer integration time. It is always possible to trade lower efficiency for faster measurements. The DC approach has an advantage over the AC approach in this respect. The AC approach has a symmetrical but additive loss of efficiency at both ends of the measurement cycle. As detailed earlier (Kunkel et al. 2001), the DC approach reduces the loss of dynamic efficiency by starting at an origin at which there is little or no loss of efficiency, cutting the loss of dynamic efficiency at least in half at each measurement site. DC measurement devices and protocols are a faster and more accurate measurement system than the AC approach. The DC approach also provides the user with a high gain device that can be used in a stationary way to measure flux oscillations in real time, which the AC system cannot do because of its limited frequency mode of measurement.

Stationary ion-selective microelectrodes can also be used to infer cellular activity but it is only applicable when large enough signals are being recorded, usually on large enough organs to generate sufficient detectable currents (e.g. roots). Vibrating or rather, as described above, stepping a microelectrode between two positions and measuring the DC voltage difference between the positions of the microelectrode greatly increases sensitivity and corrects for microelectrode drift as long as the stepping is much faster than the drift. This is particularly important when studying single or isolated cells that generate smaller currents than whole tissues or organs.

Unfortunately, the extracellular microelectrode used can only measure the ion concentration at points outside the cell wall of plants. However, the use of specific inhibitors for ion channels or transporters that putatively convey membrane fluxes provides clarification of the relative contribution of fluxes across the plasma membrane.

In a number of situations, intracellular ion concentration and its modulation by fluxes across the plasma membrane are potentially one of the earliest diagnoses of any changes that a cell displays. Therefore, the SIET has become a useful tool for the study of biological phenomena in which spatial and temporal resolution are an issue.

For reasons outside the scope of the present manuscript, the very same principle we describe here, with different instrumental interpretations, is used associated with various acronyms, namely MIFE (see Chapter 3), SERIS (see Chapter 6), and SIET here. In essence they all use the same basic relationship, the Nernst equation [1], which relates electrical potential to ionized compound concentrations. However, the DC and AC approaches diverge in technical design that sets limits or advantages for each. Self-referencing AC systems such as SERIS are based on the measurement of ion-selective microelectrode voltage differences (Nernst potentials) through a capacitor at opposite extremes of an

oscillation. The SERIS system does not directly measure the voltage on the microelectrode at each point but rather records the results in a software averaging algorithm accumulating the difference (delta V) between the two points. Though SERIS can measure the presence of a flux of an ion, it is unable to accurately measure the actual strength of the flux. The SERIS approach calibrates the electrode at low gain (DC × 10) mV sensitivity, but makes the delta microvolt measurement (gain × 1000) via a capacitor. Since efficiency of the LIX electrode is not measured at microvolt levels, it is unable to measure the flux accurately. In the AC SERIS protocol the local concentration of an ion is assumed to be close to the background media's composition (Kühtreiber and Jaffe 1990), which is a logical first guess but may not be accurate in situations where the cell is actively pumping the ion of interest. This is particularly true when dealing with $H^+$ secretion, where the local buffer concentration must be low enough for the cellular pumping to overcome it (Kunkel et al. 2001). SIET also allows sampling rules to be created for 1-, 2-, or 3-D measurements using one ion-selective microelectrode or sequential or interleaved measurements (Table 5.2) of multiple ion-selective microelectrodes in one or more dimensions (Faszewski and Kunkel 2001). SIET probes can also be interleaved with polarographic (amperimetric) microelectrodes by a sampling rule (Table 5.2) that extends the molecules measured beyond the current review's scope to non-ionic small molecules such as oxygen and nitric oxide (for an example of application see Prado et al. 2004).

This capability of measuring multiple ions is also critical to accurate estimation of certain ion fluxes. For instance, the LIX nominally used for measuring bicarbonate is primarily sensitive to carbonate which at physiological pH is a minority of ions present in the carbonate/bicarbonate equilibrium. In order to accurately measure the total carbonate/bicarbonate concentration one must also simultaneously measure local pH that is involved intimately in the equilibrium. In addition, many tip growth studies have common factors that allow correlation of the relative timing of internal and external ion movements (Holdaway-Clarke et al. 1997; Feijó et al. 1999; Roy et al. 1999). The sampling-rule approach is highly compatible with correlating the measurement of ion-selective probe data with interleaved cellular and intra-cellular data obtained from image analysis (Holdaway-Clarke et al. 1997; Feijó et al. 1999; Antoine et al. 2000, 2001, see below).

## 5.4 Capabilities of scanning microelectrode technology

In order to establish the capabilities of particular scanning microelectrode setups and analyze the data collected, we routinely use artificial ion sources or well defined model systems such as the growing pollen tube whose cylindrical shaft and hemispherical growing tip is easy to define geometrically. In that way, we can objectively test the limits of a new protocol or measurement system.

### 5.4.1 Artificial point source device

Measuring artificial sources or sinks similar to the types of currents measured in living material is a recommended first step when using this technology. Artificial ion point sources or sinks can be made using a glass capillary pulled in multiple stages to have a bee-stinger shape (Kühtreiber and Jaffe 1990). This will produce an infinite source or sink solution nearby the tip that represents the point source. This should have a tip diameter of 5–10 µm and be filled with low percentage agarose (around 0.5%) to stabilize the filling solution of the ion or molecule of interest, which should be 3 orders of magnitude higher or lower in concentration than the bathing media, thus producing a passive diffusion gradient. The agarose does not hinder the diffusion of the molecule through the tip but will stop bulk flow of the filling solution. An electrogenic flux can be simulated by a DC circuit through this source, provided that the source components are simple enough to allow the ion of interest to be a predictable component of the current. The predicted pattern of diffusing oxygen into a recessed platinum electrode surface can be seen in Fig. 5.1A, which illustrates a sagittal section through the artificial source tip and sphere of predictable oxygen concentration, according to the equations of Schneiderman and Goldstick (1978). The results of measuring the flux emanating in the three directions, x, y and z, from a point source in a grid of points in a YZ plane tangent to the sphere of molecules diffusing from a point source tip such as in Fig. 5.1A is plotted in various ways in Fig. 5.1B, E, F. Planar contour plotting functions of grid data (Fig. 5.1E) are available in many computational software packages such as MathCad, Matlab, or R. The characteristic reversals of flux components, as the probe passes high and low in the Z dimension, emanating from the source tip can also be seen in linear plots, Fig. 5.1E, of the $J_y$ data from Fig. 5.1D. A more intuitive stereo view of total flux vectors, Fig. 5.1B, C, requires use of software packages such as Mage, able to represent points in space and provide stereo pairs. It is important to be aware of the total flux vectors involved at each point measured when plotting one or two-dimensional representations (e.g. Fig. 5.8A–C) of those vectors. In some cases a vector can represent a small local 1-D component of a larger 3-D flux associated with an adjacent localized point source or sink. Familiarity with the measurement phenomena, solid geometry and distance, inherent in Fig. 5.1 is critical to understanding fluxes measured from natural sources.

For testing multiple-probe arrays, one can devise gradients of each molecule of interest emanating from a single point source. For instance, to create a joint point source for protons and carbonate and point sink for oxygen, one can craft a small capillary with gaseous $CO_2$ forced to the tip presenting a small gaseous interface that releases $CO_2$ which associates with the water to form a point source of bicarbonate, carbonate and protons. In addition, the pure $CO_2$ bubble provides an infinite sink for dissolved oxygen. This artificial source has been used for testing multi-probe pairs such as $HCO_3^-$ and protons (Faszewski and Kunkel 2001) or protons and $O_2$.

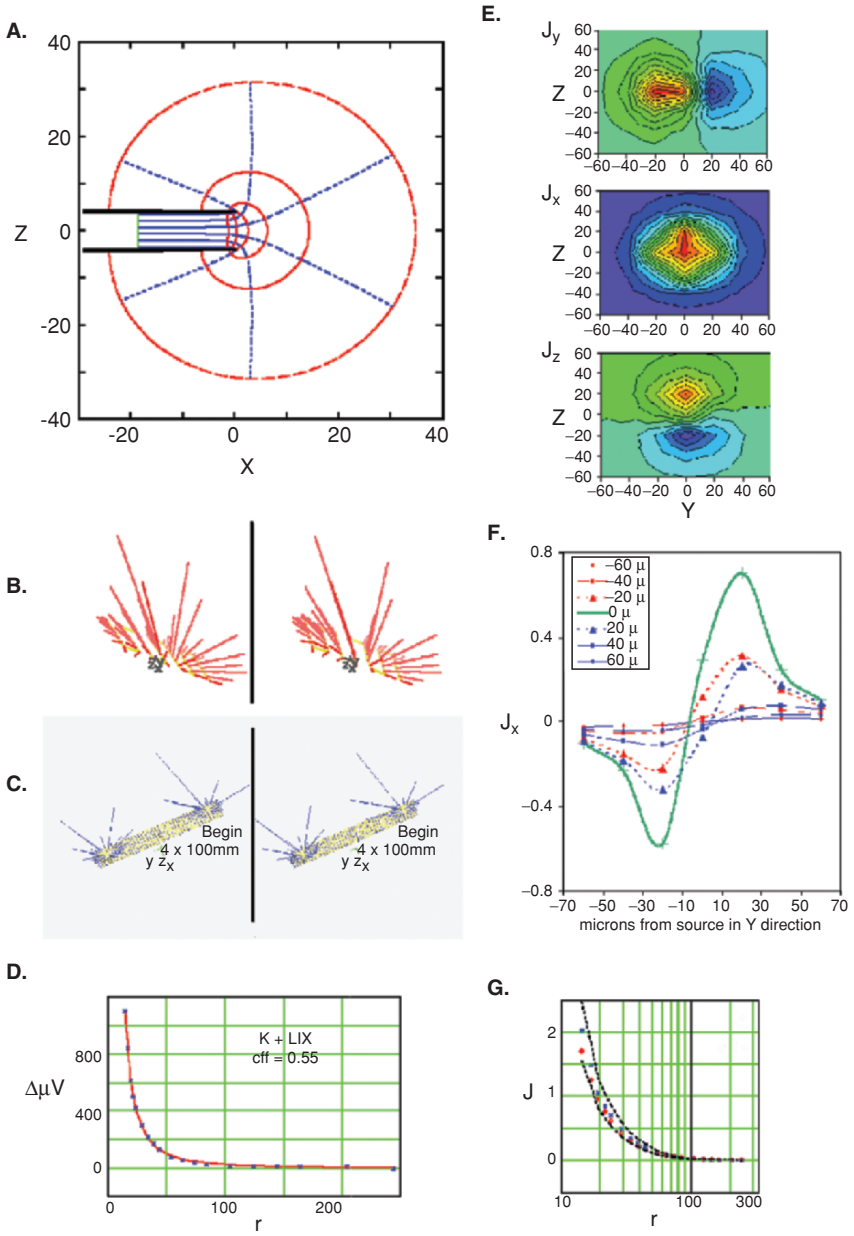


**Fig. 5.1.** Point source in theory and practice. **A** The computed pattern of oxygen diffusing into a capillary tube with a recessed platinum surface which serves as an oxygen sink. **B** Stereo image pair of calcium flux vectors emanating from a point source. **C** Stereo image pair of proton flux vectors emanating from a pair of point sources 1.5 mm separated. **D** Dynamically measured microvolt differences (ΔμV) measured at graded radial distances from a point source. The expected ΔμV was computed by extrapolation between known linear voltage versus 1/r points and multiplied by an estimate of the dynamic efficiency to attempt to fit a red line of expected

## 5.5 Calibrations of probes using particular sampling rules

Each LIX microelectrode has an efficiency of flux measurement dependant upon the time it takes to settle to a new voltage level at a new ion concentration. Calibration of a DC system in solutions of known concentration is a meaningful measurement of LIX responsiveness, and relates directly to how the electrode will be used in measuring gradients. When presented with a steady state ion flux from a point diffusion source (Fig. 5.1A), optimization requires waiting long enough at a given sample position with sufficient gain to record an accurate ion concentration measurement, and then moving to another position and re-measuring. The flux between the two points can be calculated from the values of *dC* and *dx* of equation [6] as explained below. Steady state sources are rare in live matrials, arguing for short waiting periods at each measurement point. The SIET system can record LIX microelectrode noise and drift, allowing the design of protocols to minimize them.

The two types of calibrations that must be made on each probe type before they can be used are both based on the Nernst equation: [1] one is the static calibration similar to calibrating a pH meter (Fig. 5.2A), estimating the slope, A, of the voltage versus log [$H^+$] plot using two standard solutions, a and b, [2, 3] (the same equations are valid for any other ion).

$$pH_a - pH_b = \log\left[H^+\right]_a - \log\left[H^+\right]_b = \left(mV_a - mV_b\right)/A, \tag{2}$$

$$A = \Delta mV/\Delta pH, \tag{3}$$

or a multipoint calibration by estimating the slope of the linear regression [4],

$$V = B + A \cdot \log\left[H^+\right]/eff_s \approx B + A \cdot \log\left[H^+\right], \tag{4}$$

using three or more of the standard solutions as seen in Fig. 5.2A.

The slope, A, and intercept, B, determined for the probe based on the set of standard solutions can be used to estimate future concentrations (cf. [5]) measured by that electrode within the range of the standards used:

$$\left[H^+\right] = 10^{\left(A - V * eff\right)/B} \approx 10^{(A - V)/B} \tag{5}$$

Experience shows that future replacement electrodes made with the same LIX and electrolyte backfill can be checked for an appropriate voltage with a single point calibration, namely the bathing solution in use. Thus the estimation of the

---

**Fig. 5.1.** (*Continued*) ΔμV to the observed-ΔμV (*blue x*). The guessed efficiency was adjusted to give a best fit (*red line*). **E** Contour plot of the dX, dY and dZ components of fluxes of protons eminating from a point source measured at an YZ plane about 10 microns from the tip source. **F** Linear plots of the dY data from **E** plotted against the Y location. **G** Observed flux (*blue x*) computed from the dynamic efficiency and observed ΔμV from **D**. Upper and lower 95% confidence intervals (*black dashed lines*) on the expected J (*red diamonds*) are computed from the variance of the observed about the expected ΔμV from **D**

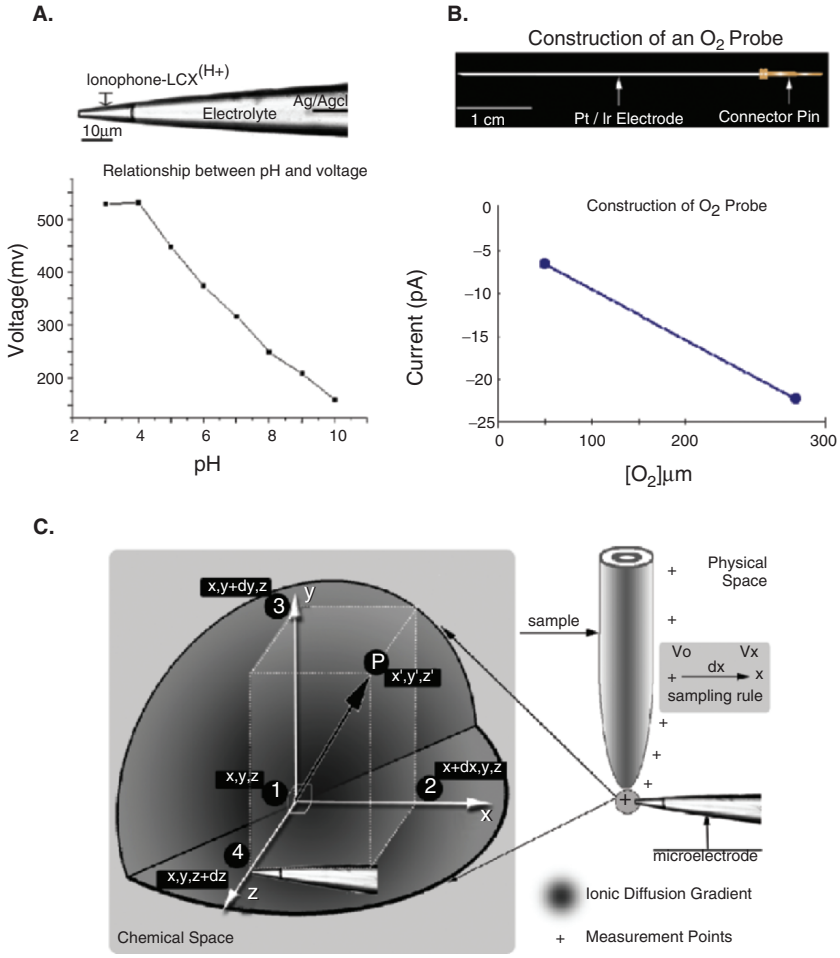


**Fig. 5.2.** $H^+$ and $O_2$ probes calibrations and sampling rules. **A** Construction and static calibration of a $H^+$ probe. Media composition for calibration was the same as pollen culture media except the pH was adjust to various values by adding either KOH or HCl. **B** Construction and calibration of an oxygen probe. The same media was bubbled with $N_2$ for over 30 min to achieve 0 µM oxygen concentration, while bubbled with air (18% $O_2$) for 30 min assumed to be 100% saturated (268 µM). **C** Sampling rules that control the movements of both $H^+$ and $O_2$ probes. At each measurement point in "physical space", both probes will make measurements from (1) ⇒ (2) ⇒ (3) ⇒ (4) ⇒ (1) in "chemical space"

concentration at the origin of a unit measurement, *Co*, is made using a static calibration curve similar to [5], for which there is close to 100% efficiency as there is with a pH meter. The other more critical calibration, in that it is less likely to be close to 100% efficient, is a dynamic calibration necessary for adequately estimating *Cx*, the concentration measured after the quick move to

position x. It depends on the LIX used and imposed sampling parameters such as the length of the LIX column, the wait before measuring and the length of the measurement phase, which jointly give rise to the probe dynamic efficiency (Fig. 5.1D). When divided into the observed microvolt difference, it allows prediction of the true microvolt difference critical to calculate the accurate flux (Fig. 5.1G).

$$J = D \cdot dC/dx = D \cdot (Cx - Co)/dx \quad (6)$$

Thus the loss due to dynamic inefficiency would show itself in the estimation of the $C_x$ component of *dC*. The probe is allowed to sit at the measurement point for a wait-state long enough for the probe to reach close to its optimum voltage (i.e. ~100% efficient) where $C_o$ is calculated using equation [5]. Then the probe is moved *dx* units to its position for measuring, $C_x$, where it is often necessary to take the voltage reading, $V_x$, (Fig. 5.2C) before the probe has come to equilibrium resulting in a loss of efficient measurement of $V_x$, underestimating the voltage. This inefficiency systematically underestimates the flux. One wants to take the $V_x$ measurement at *dx* quickly in order to avoid any drift in the probe's voltage, and also quick to allow more measurements so to better represent the true dynamics of a living source. With a stable point source, the voltage at each point, *r*, away from the source can be measured with the probe in static, 100% efficient, positions. Then, *V* versus *1/r* is plotted, a curve is fit to it and the expected voltage difference for the small extra move is calculated by interpolation between the measured points. In the same time frame as the static measurements are made, the voltage difference for a rapid *dx* move can be directly measured dynamically in real time. The difference between the measured and calculated voltage difference provides an estimate of the dynamic inefficiency of that sampling rule. This artificial source dynamic efficiency estimate provides the efficiency to use in correcting future experimental measurements of voltage differences. For a rapidly responding LIX such as the proton LIX there is almost no dynamic loss in efficiency in the measurements of the secondary voltages at *dx*, *dy* or *dz* and thus a 100% efficient estimate of a 3-D flux can be assumed (Table 5.1). This high dynamic efficiency is not true for the older continuous AC vibrating or SERIS methods, in which efficiency is lost at each end of the microelectrode oscillation, leading to further losses of efficiency for the proton electrode (Kunkel et al. 2001).

The concentration of ions diffusing from a point source such as displayed in Fig. 5.1, depend on diffusion alone and can be modeled as a hyperbola:

$$C_r = C_b + K/r, \quad (7)$$

where $C_r$ is the concentration at radius *r* and *K* is a proportionality constant which includes the diffusion coefficient; $C_b$ is the background concentration. Unfortunately, *r* is not the distance to the point source, but rather a hypothetical point up inside of the point-source-shaft that corresponds to the infinite source end of the hyperbola at which *r* is zero. This point can be esti-

mated, providing a straight-line theoretical curve of expected concentrations or microvolt differences at given diffusion radii. It is in such a context of expected μV differences that one can estimate the dynamic efficiency, $eff_d$. This dynamic efficiency is used in an equation [8] for estimating *dC*:

$$dC = C_r - C_{r+dx} = C_r - 10^{\left(mVr + \mu Vdiff/1000 * effd\right) - A)/B)}, \quad (8)$$

which can then be used to compute the flux using equation [6].

Despite the apparent mathematical sophistication, most of these equations have been introduced in simple worksheets of intuitive and simple usage and can be implemented by any inexperienced user in a matter of few hours.

## 5.6 Point sources used to test the resolution of microelectrodes

To establish the resolution of a measurement protocol and distinguish between point sources multiple sources can be created at fixed distances measured with a grid pattern (Fig. 5.1C; see also Somieski and Nagel 2001).

Measuring two molecular type sources (e.g. protons and oxygen) simultaneously presents a similar problem of resolution. The standard polarographic oxygen electrode (Fig. 5.2B) applies a steady voltage to its exposed platinum tip in order to make its measurement. The applied voltage of the oxygen electrode can interfere with an adjacent $H^+$-specific electrode (Figs 5.3, 5.4A). We quantified this interaction by measuring the oxygen electrode current and the $H^+$ electrode voltage with the two microelectrodes at different distances. While the oxygen electrode current (Fig. 5.5) is independent of the proton electrode, the proton electrode is affected by being less than 40 μm from the oxygen electrode tip.

Using a specific SIET sampling rule (Table 5.2) we were able to maintain a 40 μm distance between the two microelectrodes and sample an artificial source of protons and sink of oxygen to obtain a simultaneous measure of proton and oxygen flux (Fig. 5.4B–D). In that demonstration (Fig. 5.4B) the two contour plots of the data appear offset from one another due to the fixed distance between the two microelectrodes. By using a compensating adjustments via the sampling rules which sequentially steps the two microelectrodes to a common location while maintaining their physical distance (>35 μm apart) we are able to measure the oxygen and proton flux around the artificial source (Fig. 5.4) and the pattern of currents can be shown to be coincident. We subsequently applied this pairing of microelectrodes and sampling rule to a growing pollen tube tip (Fig. 5.6), and demonstrate the similar distribution of proton secretion and oxygen utilization in the region posterior to the growing tip known to be rich in mitochondria. This highlights the importance of studying model sources whenever multiple probes are used.

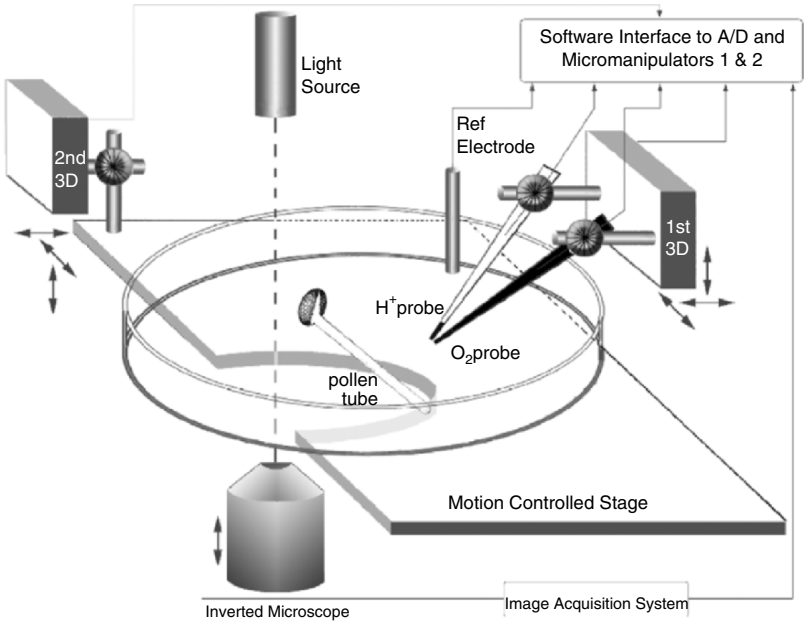


**Fig. 5.3.** Schematic diagram of multiprobe setup. $H^+$ and $O_2$ selective probes are plugged into pre-amplifiers (one a SIET and one polarographic). Both probes are mounted on a common 3D micromanipulator (*1st 3D*), by a motion controller. The pollen tube in its culture dish are held on a motion controlled stage held by a second 3D micro-manipulator (*2nd 3D*) controlled by a second motion controller which allows the rapidly growing tip to be maintained in the center of the stage. The probe amplifiers, two motion controllers and the camera are adjusted and controlled by the computer program ASET. A small drop of concentrated germinating pollen was spread evenly on the bottom of the Petri dish, which was coated with 10% poly-lysine. The 3 ml of liquid culture medium is added or changed in the Petri dish by gravity addition and maintained at a constant level by a suction skimmer

## 5.7 Different plant systems investigated

The SIET has been extensively used in a number of systems, from brown algae to higher plants, multi or unicellular systems but its use in single or isolated plant cells is of particular importance, since the currents generated are generally smaller in magnitude and therefore impossible to detect with stationary electrodes. This technique has allowed considerable advances in understanding some of these systems and therefore, we will focus on results obtained in single or isolated cells like pollen tubes (Fig. 5.7C–E; Fig. 5.8A), root hairs (Fig. 5.8D–F) and higher plant fertilization, studied through an in-vitro fusion system in maize (Fig. 5.9).

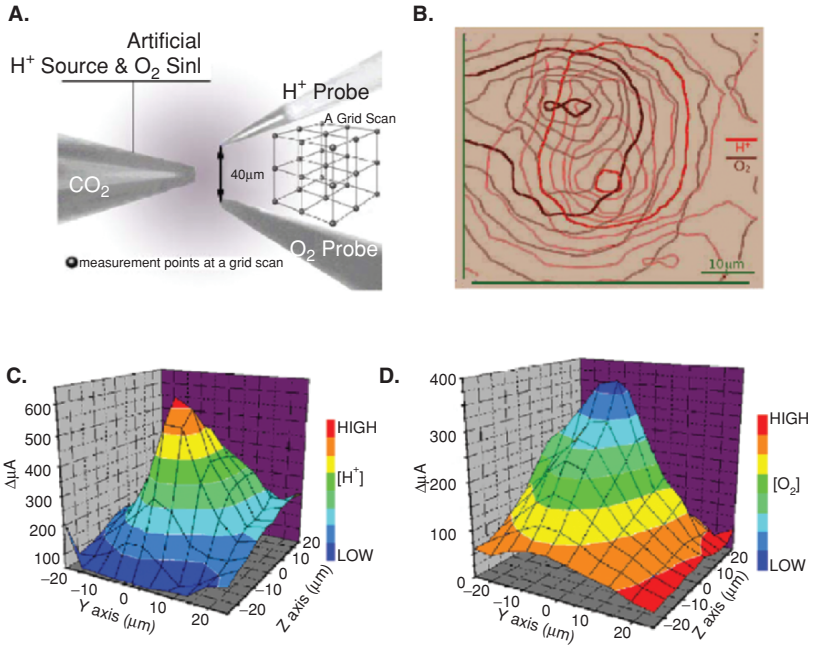


**Fig. 5.4.** No interference between $H^+/O_2$ probes using sampling rule with probes 40 µm apart. **A** Artificial dual source. A micropipette filled with $CO_2$ acts simultaneously as an $H^+$ source and $O_2$ sink. **B** Contour plot of micro-volt differences and pico-amp differences obtained from $H^+$ and $O_2$ probe readings respectively. **C** total $\mu V$-*difference* = $(\Delta\mu V_x^2 + \Delta\mu V_y^2 + \Delta\mu V_z^2)^{1/2}$ obtained from $H^+$ probe. **D** total $\mu A$-*difference* = $(\Delta\mu A_x^2 + \Delta\mu A_y^2 + \Delta\mu A_z^2)^{1/2}$ obtained from the $O_2$ probe. In both **C** and **D**, the total $\mu V$-*difference or* $\mu A$-*difference* was plotted onto the coordinate space of the probes reference position correcting for the 40 µm separation. In **B**, the contours are drawn with respect to the probes physical positions showing the 40 µm separation

## 5.8 Pollen tubes

The largest body of data acquired with extracellular, non-invasive techniques in single cells of higher plants was obtained on pollen tubes. These cells represent one of the most remarkable examples of polarized growth in nature. Since the early developments of the vibrating probe, they have been thoroughly used as a model and illustrate beautifully the potential of the technique.

Pollen tubes were first used by the group of L. Jaffe (Weisenseel et al. 1975) to demonstrate the use of the vibrating voltage probe, using germination media of ionic simplicity and low salt concentration, which yielded a high signal-to-noise ratio, and were able to demonstrate the existence of large electrical currents traversing pollen tubes, with the grain acting as the source of current and the tube as the sink. In parallel, Jaffe's group showed a common pattern in fucoid eggs undergoing tip growth, which were already known to drive electrical currents through themselves (Jaffe 1966, 1968). This similarity, albeit with huge physiological and genetic differences, suggested a causal

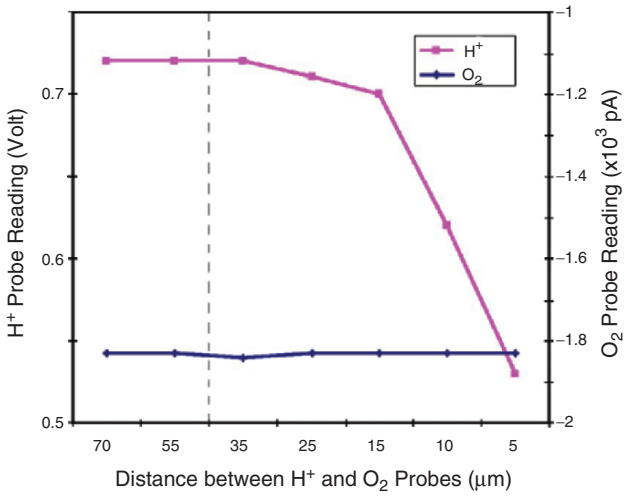


**Fig. 5.5.** Interferences between $H^+$ and $O_2$ probes. The two probes were manually adjusted to be separated by different distances while readings from both probes were collected. The media was the same as lily pollen culture media at pH 5.5, 100% air saturated. *Dotted line* indicates the recomended distance to avoid interference

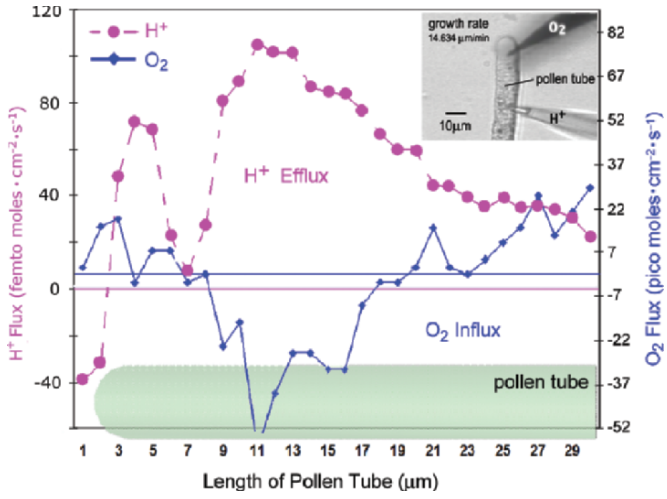


**Fig. 5.6.** $H^+$ efflux and $O_2$ influx in Z-axis plane over alkaline band region. Pollen tubes 800–2500 µm in length were selected for measurements. $H^+/O_2$ fluxes, as $\Delta\mu V_z$ and $\Delta\mu A_z$, at the surface of a pollen tube were measured by moving the electrode to within 2 µm from the tube surface. Background references were taken at least 500 µm away from any pollen grains or tubes and the value was subtracted from the surface measurements. The inset image is a screen shot showing the $H^+/O_2$ probes and a growing pollen tube with growth rate of 14.634 µm per min. This figure is a typical plot of five independent experiments

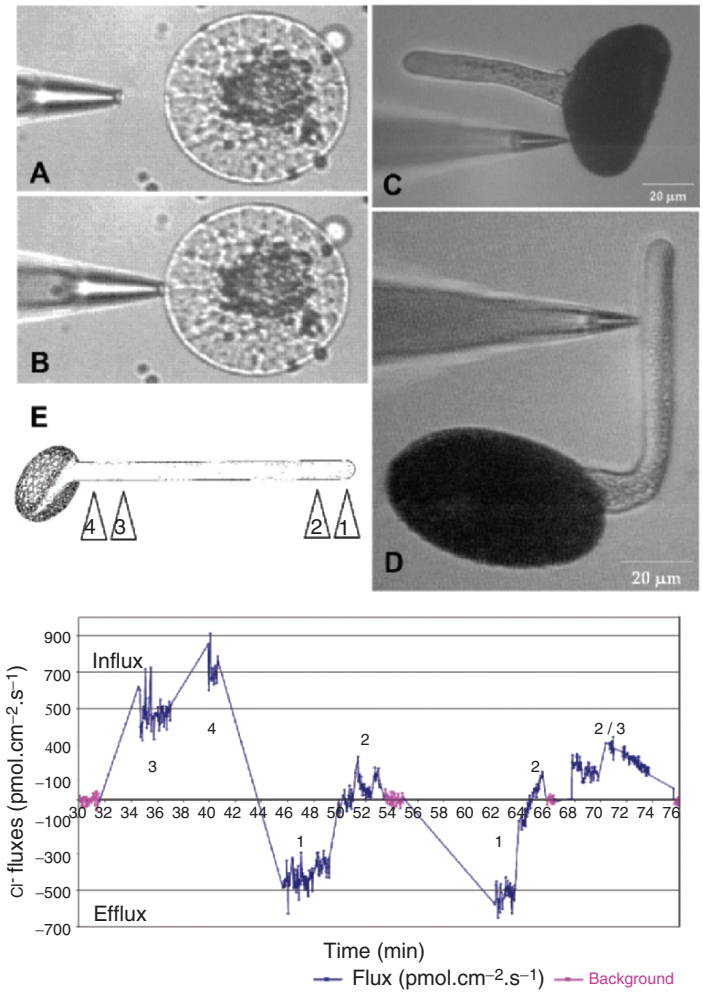


**Fig. 5.7.** **A, B** Ion-selective vibrating microelectrode recording of fluxes at the surface of an egg cell of maize before fusion (male gamete at the top right side). The microelectrode moves ("vibrates") between two positions, one away from the cell (**A**) and one close to the cell (**B**) repetitively and the delta V values are recorded. All microelectrode measurements are referred to an AgAGCl type reference electrode in the bath located far away (tens of millimetres) from the specimen. **C, D** Vibrating ion-selective microelectrode recording fluxes at the germinated pollen grain (**C**) and at the sub-apical flank of a growing pollen tube (**D**) of *Lilium longiflorum*. The ion-selective microelectrode positioning and repetitive movement is accomplished by a computer-controlled three-dimensional micro-stepping motor translation assembly providing sub-micrometer spatial resolution. **E** Chloride flux profile along a growing pollen tube of *Lilium longiflorum* between 200 and 400 µm long. The *arrows* in the scheme indicate the location of the measurements at the cell surface and correspond to the plot below. Positions *1* and *2* correspond to the apical domain and clear zone and *3* and *4* to the tube flank closer to the pollen grain

**Fig. 5.8.** **A** Extracellular proton flux profile on a growing pollen tube. The efflux region roughly corresponds to the domain occupied by the clear zone. A close correlation is observable between the cytosolic alkaline band (data not shown) and the patterns of proton efflux, suggesting that the elevation of pHc in the clear zone may correspond (at least partly) to an active proton efflux in the same area. (Adapted from Feijó et al. 1999, with permission from The Rockefeller University press.)

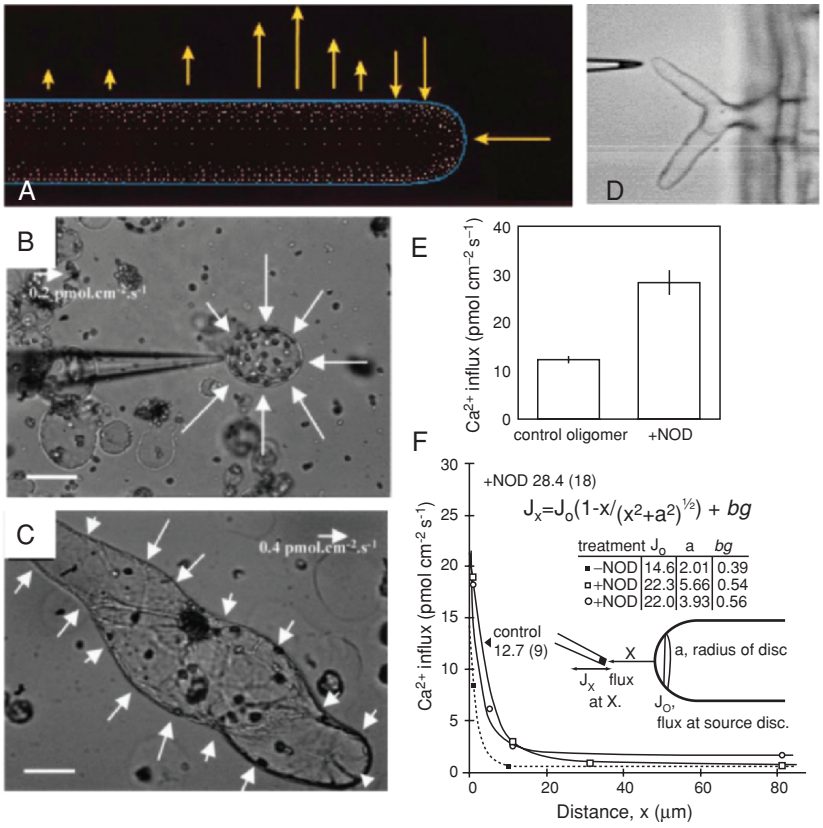


**Fig. 5.8.** (*Continued*) **B, C** Measurement of $H^+$-fluxes around elongating tobacco cells. **B** Young cell at the start of elongation, together with its pattern of proton fluxes, where the length of the arrows (scaled as indicated on the figure) is representative of the magnitude of the flux. **C** Older, well-elongated cell together with its pattern of proton fluxes. Bar=50 µm. (Adapted from Vissenberg et al. 2001, with permission from the Society for Experimental Biology.) **D** Measurement of ion fluxes in root hairs of *Arabidopsis* (in this case a *tip-1* mutant plant). **E, F** Extracellular $Ca^{2+}$ fluxes in *P. vulgaris* root hairs responding to Nod factors. **E** Bar graph of nearest approach measurements at approximately 1 µm from the root hair apical surface. Control root hair cells exposed to chitin-oligomers (structurally similar to Nod factors but biologically inactive) for 5 min had an average $Ca^{2+}$ influx at 1 µm from the tip of approximately 13 pmol $cm^{-2}$ $s^{-1}$ (*n*=9). Hairs exposed to Nod factors for 5 min on average had a higher $Ca^{2+}$ influx of approximately 28 pmol $cm^{-2}$ $s^{-1}$ 1 µm from the tip (*n*=18). Error bars are SEM. **F** Estimation of the $Ca^{2+}$ sink area at the tip of *P. vulgaris* root hairs responding to Nod factors. The graph shows step away measurements of $Ca^{2+}$ influx in the X direction, $J_x$ (in pmol $cm^{-2}$ $s^{-1}$) at distances *x*, from the root hair tip in a control hair exposed to the inactive chitin-oligomer (*filled squares*) and two hairs treated with Nod factors (*hollow squares* and *circles*). *Lines* are theoretical plots obtained with the values shown in tabular form of parameters corresponding to (a), the radius (*m*) of the $Ca^{2+}$ sink at the tip and *Jo*, the flux of $Ca^{2+}$ at the tip surface (i.e. when x=0). The best fit was obtained by iteration; minimizing a chi-square statistic while changing the influx, Jo (pmol $cm^2$ $s^1$), and radius (a) parameters individually. In the control root hair (measured in the presence of the chitin-oligomer), the best fit was obtained with a radius of 2.01 m (*dotted line*), while in the two examples responding to the Nod factors, the best fit corresponded to a sink radius of 3.93 and 5.66 m, respectively. We made measurements at five step-away positions for each root hair. *Filled arrowheads* indicate average influx values 1 µm from the tip of root hairs treated with either inactive chitin-oligomers or Nod fractors, as shown in (a), number of cells measured shown in parentheses. (Adapted from Cárdenas et al. 1999, with permission from Blackwell Science Ltd.)

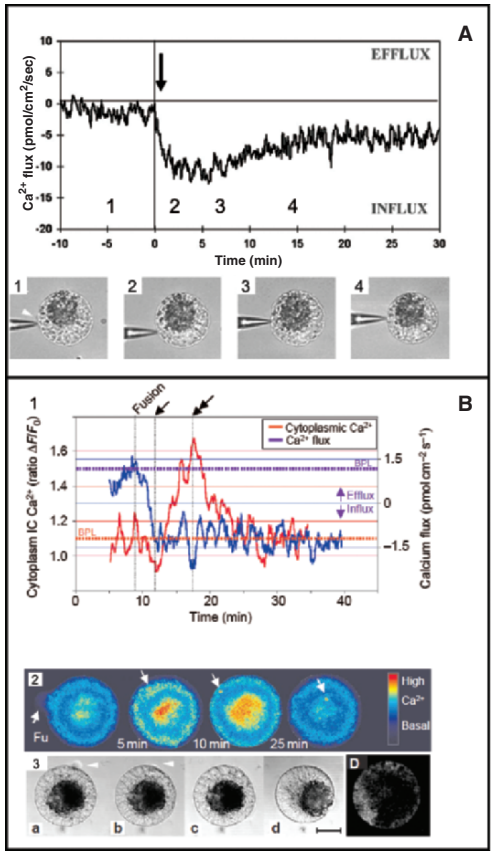


**Fig. 5.9.** **A** $Ca^{2+}$ flux measurements during maize IVF. A typical recording is shown ($n$=61) illustrating the onset of a $Ca^{2+}$ influx after fusion. Time 0 is chosen arbitrarily as the time of gametic fusion, as asserted by direct microscopic observation. The *arrow* shows the detectable onset of a $Ca^{2+}$ influx after fusion. A clear $Ca^{2+}$ influx was always detected in the egg membrane, with a delay to fusion dependence on the relative position of the probe and fusion site (*black arrow* in the plot). *1*, *2*, *3* and *4* refer to the time when the pictures (bottom) were taken. The following events are depicted: (1) egg cell before fusion (male gamete position is shown by a *white arrow*); (2) egg cell after fusion, just when contraction has started; (3) strong egg cell contraction; and (4) egg cell reshaping (adapted from Antoine et al. 2000, with permission from the National Academy of Sciences). **B** Simultaneous measurement of $Ca^{2+}$ flux and $[Ca^{2+}]_{Cyt}$ during maize IVF. (1) typical experiment ($n$=7). Time zero is set at the time when gametes have adhered (*vertical line*). Fusion is followed by the onset of a $Ca^{2+}$ influx (*blue line*; average $Ca^{2+}$ influx of −1.19±0.01 pmol $cm^{-2}$ $s^{-1}$) and by a transient increase in $[Ca^{2+}]_{Cyt}$ (*red line*). In this particular experiment, the onset of the rise in $[Ca^{2+}]_{Cyt}$ occurs when the influx stabilizes close to the maximum (*arrow*), and the peak $[Ca^{2+}]_{Cyt}$ is coincident with the peak of influx (*double arrow*). Nevertheless, this is not the rule for all the experiments; usually these two features behave without any visible correlation. *BPL* basal pre-fertilization level. (2) Sequence of typical raw images from which the line in 1 was computed. The first image shows sperm–egg cell adhesion (*arrowhead*). The sperm becomes visible after fusion because of Fluo-3 diffusion into it (*arrowheads*). Traces in (1) were computed by averaging the total egg—cell or zygote fluorescence as shown in **B** (ΔF/F0=(Ft-F0)/F0). (3) Different cytological events during maize IVF in standard conditions ($n$>100)

and general role for electrical currents in initiating and maintaining tip growth.

Their observations might have been tainted by the fact that the microelectrode vibration can affect the gradients that it is recording. The vibration frequency of the vibrating voltage microelectrode (200 cycles per second or more) was one of the major problems affecting this study. To obviate the movement that the cells would undergo due to stirring created by microelectrode vibration, these initial recordings were done using a cellophane membrane to immobilize the cells, which would otherwise be freely floating in the liquid germination media and impossible to track. This membrane does not create an electrical barrier and the recording is therefore not affected by it. However, the added distance due to the thickness of the cellophane does not match the geometry of the actual cell, creating a deformation in the electrical field as measured over the membrane.

Despite the possible artifacts, the observation that the steady currents formed a dipole in growing pollen tubes and that this was common to other cell types sharing a tip growth mechanism, was a conceptually important step. The determination of a current source and sink lead to the idea that in the developmental process of pollen tubes, membranes tends to form domains, one of which is an ion-leaky state in the sink region and the other is an ion-pumping domain in the source region. Also, it was speculated that an electrical current would therefore traverse pollen tubes, creating a loop. In turn, this could generate a movement of isolated cellular constituents that could be pulled forward by the current, since it was assumed that most are small and free enough to move through the cytoskeleton. This concept of membrane domain formation, together with the hypothesis of electrophoretic movement, was proposed as a way in which electrical currents could have important physiological consequences. The molecules in the cytosol are, however, buffered by such substantial Brownian motion energy that the actual induction of their translational movement in free solution by the ion current potentials is unlikely. A more likely hypothesis is that ion potentials could provide the orientation that provides the direction for actin or tubulin based cytoplasmic motility engines used for navigation. Another conceptually important aspect of this pioneering study was the presence of electrical currents predicting the tube germination site. This implied that electrical currents could be the basis of a morphogenetic process such as the onset of tip growth. At those early times, the currents were weak and likely

---

**Fig. 5.9.** (*Continued*) Gametes were isolated from the inbred line A188. *a* Gamete adhesion (*arrowhead* shows the sperm). *b* Fusion; the sperm can be seen penetrating the egg cell (*arrowhead*). *c* Mild contraction of the egg cell. *d* Reshaping of the cell; the organellar mass has taken a peripheral position, polarizing the zygote. **D** Two-photon microscopy section of the vacuolar zone in a typically Fluo3-AM loaded egg, showing that the vacuole and large organelles are not significantly sequestering the probe. Scale bar in bd, 20 m.) (Adapted from Antoine et al. 2001, with permission from Nature Publishing Group.)

mark the spot where an important process is to happen but are less likely to be the motive force (the quest for causal roles of currents, or ions as they move, remains at the centre of ion flux studies!).

The vibrating voltage probe did not, however, provide any information about the ionic nature of the currents. If at all, this could be inferred by changes in the composition of the medium used which can by themselves affect the physiology of the cells. Weisenseel et al. (1975), based on the dependence of current on the ionic composition of the medium, suggested that most of the inward current consisted of potassium ($K^+$) ions entering the whole pollen tube uniformly. At the growing tip, they speculated that calcium ($Ca^{2+}$) could be part of the current loop. To further examine the ionic nature of the currents, Weisenseel and Jaffe (1976) performed more media ion-substitution experiments. They implicated protons ($H^+$) as an important part of the outward current at the grain and $K^+$ as the major component of the inward current at the tube. But the development of the vibrating $Ca^{2+}$ specific ion-selective probe (Kühtreiber and Jaffe 1990) uncovered an apparent contradiction with these conclusions since a $Ca^{2+}$ influx was measured at the tip which could, by itself, account for most of the inward current. The accuracy of the results obtained with the ion-selective vibrating probe precluded previous vibrating voltage probe data from being quantitatively correct. The authors analyzed fucoid eggs, pollen, *Dyctiostelium discoideum*, amoebae, *Sarcophaga* follicles and fertilized ascidian eggs. In all of these systems, they detected $Ca^{2+}$ currents with possible roles in development.

An important constraint of the vibrating ion-selective probe technique is that the $Ca^{2+}$ specific LIX microelectrode performs better under low media calcium while not all biological material (e.g. marine) will behave normally under these conditions. Pierson et al. (1994) later confirmed $Ca^{2+}$ influx at the growing tip of pollen tubes and related the extracellular $Ca^{2+}$ influx to a tip-focused intracellular $Ca^{2+}$ gradient through the activity of putative membrane channels.

Due to the importance attributed to $Ca^{2+}$ in signaling, the first few years after the development of vibrating ion-selective microelectrodes were devoted to $Ca^{2+}$ flux studies.

An important feature of the growth of pollen tubes of most species studied lies in the fact that tip growth is at some point oscillatory. Following Weisenseel et al.'s (1975) observation that total currents at the tip of growing pollen tubes were pulsatile after a certain tube length, Holdaway-Clarke et al. (1997) showed that $Ca^{2+}$ was a part of this pulsatile component. $Ca^{2+}$ influx oscillates and this correlates with the growth oscillations. Yet $Ca^{2+}$ influx is delayed by 13 s relative to the growth pulse and seems to be secondary to growth oscillation. The reasoning that allows this inference is based on the strength of the cross-correlation when the phase of the oscillating components is shifted relative to one another (Holdaway-Clarke et al. 1997). Reasons for this delay have been proposed to reside on buffering capacity of the cell wall (Holdaway-Clarke et al. 1997) or a mechanism involving turgor

pressure (Messerli et al. 2000). Messerli and Robinson (2003) further tried to test these two models, by changing the growth medium's ionic composition and recording changes as a function of ion fluxes. They concluded that none is sufficiently robust to account for the experimental data.

When measuring ion fluxes and assessing the space and time correlation to growth, it is important to correlate these with the cytosol concentrations of the ion being studied. We have studied the contribution of protons to the tip growth process (Feijó et al. 1999), and demonstrated a tight correlation between the intracellular distribution pattern and the fluxes across the membrane. The pattern involves an influx of protons at the growing tip corresponding to an acidic domain in the cytosol and an efflux in the region that corresponds to the clear zone and to an intracellular constitutive alkaline zone (Fig. 5.8A). Whether the two are mechanistically related remains a matter of debate.

Messerli et al. (1999) reported oscillations in $H^+$, $K^+$ and $Ca^{2+}$ fluxes at the growing tip, all lagging the growth pulses but failed to detect the efflux region of protons on the clear zone. However, the use of substantial amounts of buffer concentration in the medium by these authors (5 mM MES buffer, compared to 0.05 mM MES) is known to affect the measurement of $H^+$ gradients in a sufficient manner to mask these effluxes beyond detection (Kunkel et al. 2001). $H^+$ effluxes on the sub-apical area of pollen tubes had been previously measured in pollen tubes (Feijó et al. 1999), and correlated with the distribution of proton-pumping ATPases (Certal et al., unpublished data).

This later example argues that careful medium design for recording with particular microelectrodes is needed whenever applying ion-selective microelectrode measurement systems. Media should be ionically as simple as possible, especially with regard to the ion being measured, in order to increase the signal-to-noise ratio to record small signals. This technique records a specific concentration at each point of the measurement algorithm in the extracellular medium. A change in concentration implies a flux. When dealing with $H^+$, it is essential to think about the buffer used and its concentration and to test how this affects the measurement. Ideally, buffer concentrations should be kept as low as possible, so as not to interfere, since buffers will absorb protons and therefore, deflate the extension of concentration gradients (Kunkel et al. 2001).

Messerli et al. (1999) acknowledge that buffering has an effect on the measurement and they correct the flux values obtained according to previously determined correction factors (Arif et al. 1995; Demarest and Morgan 1995), however, do not account for the possibility that this not only affects the magnitude of $H^+$ fluxes but it might also alter the extracellular gradients such that some fluxes are no longer measurable. Kunkel et al. (2001) showed that several complications result from using pH buffers in the medium where proton-specific LIX microelectrodes are used. Facilitated diffusion enhances the measured $H^+$ flux due to proton equilibration with the buffer. The buffer absorbs local $H^+$, allowing them to escape the source more rapidly than by

simple diffusion, enhancing proton fluxes. The major conclusion from this study is to keep the culture media as simple as possible and reduce any buffer components to as low titer as possible.

Zonia et al. (2001, 2002) subsequently showed, for the first time, that chloride ($Cl^-$)efflux cycles at the growing tip, coupled- to and in-phase with cycles of growth, indicating that $Cl^-$ dynamics is an important component in the network of events that regulate pollen tube homeostasis and growth. The rest of the tube exhibits $Cl^-$ influx (Fig. 5.7E). Pharmacological studies revealed a correlation between $Cl^-$ efflux at the growing tip and growth, and that $Cl^-$ appeared intimately associated with the control of water flow. Care was taken to avoid affects by the chemicals used in this study on the $Cl^-$-selective microelectrodes. Among the $Cl^-$ channel inhibitors that have an effect on pollen tube growth, only DIDS was used since it was found not to interfere with sensitivity or selectivity of $Cl^-$-selective micro-electrodes. Moreover, the authors, upon realization of this unexpected result, performed the necessary controls to ensure the validity of the $Cl^-$ flux calculations. Tests were conducted in which the dynamic responses of $Cl^-$-selective microelectrodes measuring an artificial $Cl^-$ flux source were calculated to be 3 orders of magnitude higher than the other anions tested. Knowing that other anions can interfere with the measurement of $Cl^-$ anions, they calculated $Cl^-$ concentration in an alternative manner using a colorimetric assay. The results were consistent with those obtained with the $Cl^-$-selective microelectrodes.

Messerli et al. (2004) argue that the fluxes measured were in fact changes in the concentration of the anionic form of the pH buffer (MES) and not changes in $Cl^-$ concentration. In this study, the authors characterized the ionophore cocktails previously used by Zonia et al. (2002) and claim that the selectivity and possibly interference from other anions and chemicals used for chloride channel blocking would preclude the results previously obtained. However, using the buffer concentration that Zonia et al. (2002) use, Messerli et al. (2004) shows only a 3.38% reduction in potential responses to chloride concentration for a background concentration of chloride between 0.1 and 1.0 mM and 9.98% for a background concentration between 1 and 10.0 mM. Furthermore, on discussing their quantitative conclusions, these authors frequently confuse the results obtained by Zonia et al. (2002) from tobacco with the results from Lily.

This later controversy shows that when dealing with indirect evidence (such as extra-cellular concentration recordings to infer membrane fluxes), care needs be taken to ensure the validity and accuracy of the measurements. In this case, technical controls by Messerli et al. (2004) actually confirm the applicability of the technique under the conditions used by Zonia et al. (2002). Nevertheless, the controls performed show that each ionophore cocktail (LIX) used to produce an ion-selective microelectrode can not be applied universally and this example provides a model for the sorts of cautions that must be observed when testing a new ionophore cocktail or when a medium composition change or pharmacology is designed.

While it is generally agreed that healthy pollen tube growth is linked to coordinated entry of $Ca^{2+}$ and other ions at the growing tip, the coordination of entry or exit in other regions is less documented. Best understood is perhaps the $H^+$ secretion in the region of the alkaline band, which may be associated with the mitochondrial rich zone and functionally related to secretion of $H^+$ accumulated in the cytosol from active mitochondrial respiration (Feijó et al. 1999). In addition, inactivation of pollen growth by incompatibility reactions has been linked to $Ca^{2+}$ entry along the pollen tube shaft (Franklin-Tong et al. 2002).

## 5.9 Root hairs

Root hairs are highly specialized tip growing cells (Fig. 5.8D). $Ca^{2+}$ dynamics was studied using the $Ca^{2+}$-selective vibrating probe by Schiefelbein et al. (1992), who detected a $Ca^{2+}$ influx at the tip of growing root hair cells, but no fluxes at the sides or at the tip of non-growing root hair cells. Nifedipine, a $Ca^{2+}$ channel blocker, confirmed the link between growth and the $Ca^{2+}$ flux since its application inhibits both. Later, Felle and Hepler (1997) confirmed this $Ca^{2+}$ influx by imaging cytosolic $Ca^{2+}$ concentration. $H^+$ secretion by root tips has also been demonstrated by imaging external pH indicators (Jaillard et al. 1996) and this technology promises to allow flux calculations and applicability for studies of more localized cellular phenomenon (Tang et al. 2004).

Nod factors, which are lipochitin-oligosaccharides produced by bacteria in response to flavonoids present around roots, induce many processes associated with root nodule morphogenesis on host plants. Root hairs respond rapidly to these molecules and among the most rapid responses described are those involving changes in membrane potential and ions such as $Ca^{2+}$, $Cl^-$ and $H^+$ (reviewed by Cardenas et al. 2000). Allen et al. (1994) first detected changes in the extracellular $Ca^{2+}$ flux outside the root hairs after exposure to Nod factors using a $Ca^{2+}$-selective vibrating probe. Cardenas et al. (1999) further determined that these changes occur within the first 5–10 min of Nod factor application (Fig. 5.8E,F). A sharp increase in the $Ca^{2+}$ influx level (from 12.7±0.7 to 28.4±2.8 $pmol.cm^{-2}.s^{-1}$) at the tip of root hair cells occurs concomitantly with an increase of the membrane area over which the influx occurs and with an increase in the concentration of the intracellular free ion. Technically, this study clearly showed the importance of using a protocol that estimates both the intensity and the area of current production, since the NOD induced increase of total $Ca^{2+}$ flux at the root hair tip (Fig. 5.8F) is composed of both an increase in intensity as well as the area over which the flux occurs. This objective can be accomplished by either a scan of the source area close to the cell or doing a step-away measurement of the declining signal with distance (Fig. 5.8F).

As for $H^+$, although fluxes have been implicated in root hair growth and Nod factor response, only stationary ion-selective microelectrodes have been

used and the results were apparently contradictory. The pH around the root hair remains acidic, but becomes less so in response to Nod factors. Since intracellular pH increases, this alkalinization could be expected to correspond to an acidification of the extra-cellular medium so it is not clear why the intra- and extracellular changes occur in the same direction. Felle et al. (1998) justifies this by considering different buffering capabilities of the intra and extra-cellular compartments. Cardenas et al. (2000) also argue that, based on data from stationary ion-selective microelectrodes and scanning $H^+$-selective microelectrodes along the whole root, the complexity of $H^+$ regulation is likely to be the result of a system more elaborate than just two compartments with different buffering properties.

## 5.10 Fertilization in higher plants

More recently, the SIET contributed to a major breakthrough in plant development, when a study by Antoine et al. (2000) made a direct measurement of an influx of extracellular $Ca^{2+}$ induced by gamete fusion in maize (Fig. 5.9). The extracellular fluxes measured at the surface of isolated egg cells, with or without adhesion of a male sperm cell were close to zero and stable over time. However, after gamete fusion, a $Ca^{2+}$ influx was triggered close to the site of sperm entry with a delay of 1.8 ± 0.6 s (Fig. 5.9A). This influx spread throughout the whole cell, progressing at a rate of 1.13 $\mu m.s^{-1}$. After this wave front propagation, the $Ca^{2+}$ influx intensity remained sustained, monotonic and homogeneous over the whole egg cell (average influx of 14.92 $pmol.cm^{-2}.s^{-1}$ lasting an average of 24.4 min). This characteristic influx, and the necessary channel opening, was shown to be the first embryonic event following and triggered by gamete membrane fusion. The cytological modifications observed after fertilization correlate well with the spread of the $Ca^{2+}$ influx and the latter changes in cytosolic $Ca^{2+}$ concentration may work as a trigger and possibly a space and time coordinator of many aspects of egg activation. It was shown that the $Ca^{2+}$ influx has a determinant contribution, since application of a $Ca^{2+}$ ionophore mimics some aspects of egg activation. Furthermore, the nature of the channels involved was assessed with the use of gadolinium ($Gd^{3+}$), which inhibited the influx, possibly implicating mechano-sensitive channels. In all species studied, gamete fusion triggers an increase in cytosolic $Ca^{2+}$ concentration. This is accepted as part of the initial steps to egg activation, but the source and regulation of this $Ca^{2+}$ signal and the way it is transduced inside the zygote are controversial. It was already known that after gamete fusion there was a rise in cytosolic $Ca^{2+}$ (Digonnet et al. 1997), sufficient for egg activation, but the relationship between this and the wave front spread of $Ca^{2+}$ influx from the fusion site was unknown. Antoine et al. (2001) addressed this question by simultaneously recording $Ca^{2+}$ fluxes and cytosolic $Ca^{2+}$ concentration, using a setup that combines the SIET and

ion-ratiometric widefield imaging. Under these conditions, it was possible to discriminate between the contribution of the cytoplasmic $Ca^{2+}$ and $Ca^{2+}$ influx. This unique technical combination allowed for the conclusion that the $Ca^{2+}$ influx precedes the cytoplasmic $Ca^{2+}$ elevation by 40–120 s, thus implicating the existence of separate mechanisms for both of these $Ca^{2+}$ signals (Fig. 5.9B). Further pharmacology and buffer suppression of the cytoplasmic $Ca^{2+}$ showed that its elevation is essential for egg activation, as measured by the initiation of cell wall deposition. However, the extracellular influx does not seem to be a necessary condition for egg activation. The inhibition of this influx does, however, prevent the sperm incorporation and consequent karyogamy, showing that both mechanisms should be combined to achieve eventual fertilization. Furthermore, it was shown that a $Gd^{3+}$-independent calcium influx is always present in the sperm plasma membrane after fusion, which might implicate a second type of calcium channel involved in the early activation steps of zygote formation.

## 5.11 Conclusions

It is clear that the scanning ion selective technique, SIET, is a powerful tool for cell biological research that has been effectively applied to various plant systems. Application of this technique requires a logical and methodical development of confidence in the tool by using model steady state sources on which to test out and calibrate the probes, after which the application to living systems can provide a rich data structure that can lead to breakthroughs in the understanding of cell growth and development if and when they have an ionic basis.

*Acknowledgements.* J.A.F.'s laboratory is supported by FCT grants POCTI/BCI/41725/2001, POCTI/BCI/46453/2002, POCTI/BIA-BCM/60046/2004 and POCTI/BIA-BCM/61270/2004. J.G.K.'s laboratory is partially supported by Applicable Electronics Inc.

## References

Allen NS, Bennett MN, Cox DN, Shipley A, Ehrhardt DW, Long SR (1994) Effects of Nod factors on alfalfa root hair $Ca^{++}$ and $H^{+}$ currents and on cytoskeletal behavior. *In:* Daniels MJ, Downie JA, Osbourn AE (eds) Advances in molecular genetics of plant–microbe interactions, vol 3. Kluwer Academic, Netherlands

Antoine AF, Faure JE, Cordeiro S, Dumas C, Rougier M, Feijo JA (2000) A calcium influx is triggered and propagates in the zygote as a wavefront during in vitro fertilization of flowering plants. Proc Natl Acad Sci USA 97:10643–10648

Antoine AF, Faure JE, Dumas C, Feijo JA (2001) Differential contribution of cytoplasmic $Ca^{2+}$ and $Ca^{2+}$ influx to gamete fusion and egg activation in maize. Nature Cell Biol 3:1120–1123

Arif I, Newman IA, Keenlyside N (1995) Proton flux measurements from tissues in buffered solution. Plant Cell Environ 18:1319–1324

Blatt M (ed) (2004) Membrane transport in plants. Ann Plant Rev, vol 15. Blackwell, London
Cardenas L, Feijo JA, Kunkel JG, Sanchez F, Holdaway-Clarke T, Hepler PK, Quinto C (1999) Rhizobium nod factors induce increases in intracellular free calcium and extracellular calcium influxes in bean root hairs. Plant J 19:347–352
Cardenas L, Holdaway-Clarke TL, Sanchez F, Quinto C, Feijo JA, Kunkel JG, Hepler PK (2000) Ion changes in legume root hairs responding to Nod factors. Plant Physiol 123:443–452
Demarest JR, Morgan JLM (1995) Effect of pH buffers on proton secretion from gastric oxyntic cells measured with vibrating ion-selective microelectrodes. Biol Bull 189:219–220
Digonnet C, Aldon D, Ledue N, Dumas C, Rougier M (1997) First evidence of a calcium transient in flowering plants at fertilization. Development 124:2867–2874
Faszewski EE, Kunkel JG (2001) Covariance of ion flux measurements allows new interpretation of *Xenopus laevis* oocyte physiology. J Exp Zool 290:652–661
Feijó JA, Malhó RM, Obermeyer G (1995) Ion dynamics and its possible role during in vitro pollen germination and tube growth. *Protoplasma* 187:155–167
Feijó JA, Sainhas J, Hackett GR, Kunkel JG, Hepler PK (1999) Growing pollen tubes possess a constitutive alkaline band in the clear zone and a growth-dependent acidic tip. J Cell Biol 144:483–496
Feijó JA, Sainhas J, Holdaway-Clarke T, Cordeiro MS, Kunkel JG, Hepler PK (2001) Cellular oscillations and the regulation of growth: the pollen tube paradigm. Bioessays 23:86–94
Feijó JA, Costa SS, Prado AM, Becker JD, Certal AC (2004) Signalling by tips. Curr Opin Plant Biol 7:589–598
Felle HH, Hepler PK (1997) The cytosolic $Ca^{2+}$ concentration gradient of *Sinapis alba* root hairs as revealed by $Ca^{2+}$-selective microelectrode tests and fura-dextran ratio imaging. Plant Physiol 114:39–45
Felle HH, Kondorosi E, Kondorosi Á, Schultze M (1998) The role of ion fluxes in Nod factor signalling in *Medicago sativa*. Plant Journal 13:455–463
Franklin-Tong VE, Holdaway-Clarke TL, Straatman KR, Kunkel JG, Hepler PK (2002) Involvement of extracellular calcium influx in the self-incompatibility response of *Papaver rhoeas*. Plant J 29:333–345
Harold FM, Caldwell JH (1990) Tips and currents: electrobiology of apical growth. In: Heath IB (ed) Tip growth in plant and fungal cells. Academic Press, New York
Holdaway-Clarke TL, Hepler PK (2003) Control of pollen tube growth: role of ion gradients and fluxes. New Phytologist 159:539–563
Holdaway-Clarke TL, Feijo JA, Hackett GR, Kunkel JG, Hepler PK (1997) Pollen tube growth and the intracellular cytosolic calcium gradient oscillate in phase while extracellular calcium influx is delayed. Plant Cell 9:1999–2010
Holdaway-Clarke TL, Weddle NM, Kim S, Robi A, Parris C, Kunkel JG, Hepler PK (2003) Effect of extracellular calcium, pH and borate on growth oscillations in *Lilium formosanum* pollen tubes. J Exp Bot 54:65–72
Jaffe LF (1966) Electrical currents through the developing fucus egg. PNAS 56:1102–1109
Jaffe LF (1968) Localization in the developing Fucus egg and the general role of localizing currents. Adv Morphog 7:295–328
Jaffe LF, Levy S (1987) Calcium gradients measured with a vibrating calcium-selective electrode. Proc IEEE/EMBS Conf 9:779–781
Jaillard B, Ruiz L, Arvieu JC (1996) pH mapping in transparent gel using color indicator videodensitometry. Plant Soil 183:1–11
Kühtreiber WM, Jaffe LF (1990) Detection of extra-cellular calcium gradients with a calcium-specific vibrating electrode. J Cell Biol 110:1565–1573
Kunkel JG, Lin L-Y, Xu Y, Prado AMM, Feijó JA, Hwang PP, Hepler PK (2001) The strategic use of Good buffers to measure proton gradients about growing pollen tubes. In: Geitman A (ed) Cell biology of plant and fungal tip growth. IOS Press, Amsterdam, 14 pp
Messerli MA, Robinson KR (2003) Ionic and osmotic disruptions of the lily pollen tube oscillator: testing proposed models. Planta 217:147–157

Messerli MA, Danuser G, Robinson KR (1999) Pulsatile influxes of $H^+$, $K^+$ and $Ca^{2+}$ lag growth pulses of *Lilium longiflorum* pollen tubes. J Cell Sci 112:1497–1509

Messerli MA, Creton R, Jaffe LF, Robinson KR (2000) Periodic increases in elongation rate precede increases in cytosolic $Ca^{2+}$ during pollen tube growth. Dev Biol 222:84–98

Messerli MA, Smith PJ, Lewis RC, Robinson KR (2004) Chloride fluxes in lily pollen tubes: a critical reevaluation. Plant J 40:799–812

Pierson ES, Miller DD, Callaham DA, Shipley AM, Rivers BA, Cresti M, Hepler PK (1994) Pollen tube growth is coupled to the extracellular calcium ion flux and the intracellular calcium gradient: effect of BAPTA-type buffers and hypertonic media. Plant Cell 6:1815–1828.

Pina C, Pinto F, Feijó JA, Becker JD (2005) Gene family analysis of the *Arabidopsis* pollen transcriptome reveals novel biological implications for cell growth and division control and gene expression regulation. Plant Physiol 138:744–756

Prado AM, Porterfield DM, Feijo JA (2004) Nitric oxide is involved in growth regulation and re-orientation of pollen tubes. Development 131:2707–2714

Roy SJ, Holdaway-Clarke TL, Hackett GR, Kunkel JG, Lord EM, Hepler PK (1999) Uncoupling secretion and tip growth in lily pollen tubes: evidence for the role of calcium in exocytosis. Plant J 19:379–386

Sanders D, Bethke P (2000) Membrane transport. In: Buchanan B, Gruissem W, Jones R (eds) Biochemistry and molecular biology of plants. ASPB, Rockville, Maryland, p 128

Schiefelbein JW, Shipley AM, Rowse P (1992) Calcium influx at the tip of growing root-hair cells of *Arabidopsis thaliana*. Planta 187:455–459

Schneiderman G, Goldstick TK (1978) Oxygen electrode design criteria and performance characteristics: recessed cathode. J Appl Physiol 45:145–154

Shipley AM, Feijó JA (1999) The use of the vibrating probe technique to study steady extracellular currents during pollen germination and tube growth. In: Cresti M, Cai G, Moscatelli S (eds) Fertilization in higher plants: molecular and cytological aspects. Springer, Berlin Heidelberg New York, pp 235–252

Somieski P, Nagel W (2001) Measurement of pH gradients using an ion-sensitive vibrating probe technique (IP). Pflugers Arch 442:142–149

Taiz L, Zeiger E (2002) Plant physiology. Sinauer, Sunderland, Mass., USA, pp 87–108

Tang C, Drevon JJ, Jaillard B, Souche G, Hinsinger P (2004) Proton release of two genotypes of bean (*Phaseolus vulgaris* L.) as affected by N nutrition and P deficiency. Plant Soil 260:59–68

Vissenberg K, Feijo JA, Weisenseel MH, Verbelen JP (2001) Ion fluxes, auxin and the induction of elongation growth in *Nicotiana tabacum* cells. J Exp Bot 52:2161–2167

Weisenseel MH, Jaffe LF (1976) The major growth current through lily pollen tubes enters as $K^+$ and leaves as $H^+$. Planta 133:1–7

Weisenseel MH, Nucitelli R, Jaffe LF (1975) Large electrical currents traverse growing pollen tubes. J Cell Biol 66:556–567

Zonia L, Cordeiro S, Feijó JA (2001) Ion dynamics and the control of hydrodynamics in the regulation of pollen tube growth. Sexual Plant Reprod 14(1–2):111–116

Zonia L, Cordeiro S, Tupy J, Feijo JA (2002) Oscillatory chloride efflux at the pollen tube apex has a role in growth and cell volume regulation and is targeted by inositol 3,4,5,6-tetrakisphosphate. Plant Cell 14:2233–2249